

## **Ground Penetrating Radar Evaluation for Flexible Pavement Thickness Estimation**

Imad L. Al-Qadi  
Charles E. Via, Jr. Professor of Civil and Environmental Engineering,  
Leader, Roadway Infrastructure Group  
200 Patton Hall  
Virginia Tech  
Blacksburg, VA 24061-0105  
Tel: 540 231-5262, Fax: 540 231-7532  
e-mail: [alqadi@vt.edu](mailto:alqadi@vt.edu)

Samer Lahouar  
Graduate Research Assistant  
3500 Transportation Research Plaza  
Virginia Tech  
Blacksburg, VA 24061-0536  
Tel: 540 231-1588, Fax: 540 231-1555  
e-mail: [slahouar@vt.edu](mailto:slahouar@vt.edu)

Amara Loulizi  
Research Scientist  
3500 Transportation Research Plaza  
Virginia Tech  
Blacksburg, VA 24061-0536  
Tel: 540 231-1504, Fax: 540 231-1555  
e-mail: [amlouliz@vt.edu](mailto:amlouliz@vt.edu)

**Virginia Tech Transportation Institute  
Virginia Tech  
Blacksburg, Virginia**

## Ground Penetrating Radar Evaluation for Flexible Pavement Thickness Estimation

I. L. Al-Qadi, S. Lahouar, and A. Loulizi

### ABSTRACT

Ground penetrating radar (GPR) technology has been used for the past 30 years for a variety of applications to assess pavement performance and structure. After all this time, the main issue remains: “How well does GPR work and under what conditions?” Results show that GPR works well for some situations, but is not an appropriate tool for other situations. It is currently not used on a routine basis by the Departments of Transportation (DOTs) in the U.S. due mainly to difficulties encountered in data interpretation, as well as the expenses involved for conducting GPR surveys. Data interpretation difficulties are mainly attributed to the fact that images obtained from the reflected signals are dependent on the GPR frequency used and the dielectric properties of the structural materials. To calibrate GPR systems and to better interpret collected data (signals), a project is currently underway at the Virginia Smart Road in Southwest Virginia. These experimental sections provide a unique opportunity to explore the feasibility of using GPR to assess pavements and to verify its practicality. The GPR system cannot detect layer interfaces unless a significant contrast in the dielectric constants exists between the two considered layers. This requirement is more important for the deeper interfaces because of material loss that further attenuates the GPR electromagnetic signals. To overcome the inaccuracy in results from time domain analyses, a more sophisticated technique is considered in this study. Preliminary results of analyzed data collected from interstate I-81 revealed an error of 6.8%, whereas the classic time domain technique showed an error of 12.7% for the same data.

## INTRODUCTION

Ground Penetrating Radar (GPR) was used for the last 30 years as a nondestructive evaluation (NDE) technique to evaluate and assess pavement structures and performance. This technique is simply based on sending electromagnetic waves through the surveyed structure and then recording the reflected signals, which occur at dielectric discontinuities of the structure. Accurate analysis of the reflected signals leads to the detection of any changes in the subsurface and the estimation of their locations and dimensions.

Depending on the application, researchers reported varied GPR performance. For pavement thickness estimation several studies were conducted (1-4). Maser (3) reported a thickness accuracy of  $\pm 7.5\%$  for hot-mix asphalt (HMA) layers ranging from 51 to 500-mm thick, and  $\pm 12\%$  for granular base layers ranging from 150 to 330-mm thick. In that study, the performance evaluation of the GPR was based on the comparison between the thicknesses predicted from the GPR data and the thicknesses measured from cores. Lahouar et al. (4) reported an average error of 6.8% for estimating the thickness of the HMA layers of an old pavement on interstate I-81 using GPR. Some studies showed the success of GPR for void detection under concrete pavements (5) whereas others showed its failure. Sheftick and Bartoski (6) reported that three short-pulse GPR systems, from different manufacturers, were used at the Pennsylvania Transportation Institute's test track to locate six artificially created voids. The study results showed that none of the three GPR personnel were able to locate the voids, and at least one of the three radar operators identified a void where none existed. As part of SHRP H-103, a similar study was conducted at the Pennsylvania Transportation Institute's test track by Al-Qadi in the late 1980s to detect voids underneath concrete pavements (some filled with water) using three different GPR systems, again without success. Al-Qadi (7) was able to measure moisture in HMA using laboratory-set focused antenna at high microwave frequency. Rmeili et al. (8) reported the success of GPR in detecting excess moisture in HMA layers, which usually leads to layer stripping. In the study, the GPR performance was evaluated by contrasting the GPR results to visual inspection of cores extracted from the surveyed road. Al-Qadi et al. (9) showed that GPR could be used to evaluate the effectiveness of geosynthetic as a moisture barrier in flexible pavements, and Loulizi et al. (10) showed the feasibility of using GPR to evaluate the effectiveness of geosynthetic when used as a layer separator to prevent migration of fines between layers.

In most of the studies on the performance evaluation of GPR, a limited set of cores are extracted from the surveyed sections. These cores are usually not representative of the whole pavement structure unless a large number is available. In most studies information on the surveyed pavement system is usually limited. This lack of information further degrades the performance evaluation results. Hence, GPR performance evaluation is not always reliable.

These shortcomings in the performance evaluation of GPR systems were addressed at the Virginia Smart Road, which offers a unique opportunity to explore the feasibility of using GPR to accurately measure layer thickness and monitor pavement performance over time. This paper presents a summary of the ongoing GPR research conducted at the Virginia Smart Road, and aims to evaluate the performance of an air-coupled GPR system.

## THE VIRGINIA SMART ROAD

The Virginia Smart Road in Southwest Virginia is a unique, state-of-the-art, full-scale research facility for pavement research and evaluation of Intelligent Transportation Systems (ITS). When completed, the Virginia Smart Road will be a 9.6 km (6 mile) connector highway between Blacksburg and I-81 in Southwest Virginia. The first 3.2 km (2 miles) has already been constructed, and is designated as a controlled test facility. This connection will serve an important role in the I-81/I-73 transportation corridor. After construction, provisions will be made to route traffic around controlled test zones on the Virginia Smart Road to allow for ongoing testing.

The Virginia Smart Road test facility has 12 flexible pavement sections and a continuously reinforced concrete pavement section. The flexible pavement sections were heavily instrumented (using approximately 500 sensors) during construction to allow pavement performance monitoring under real vehicular loading and environmental conditions (11). The sensor array includes different types of strain gages (to measure longitudinal and transversal strain), pressure cells (to measure vertical stress), thermocouples, time-domain reflectometry (TDR) probes (to measure moisture content), and resistivity probes (to measure frost depth). These sensors provide continuous data for the different parameters of interest underneath each pavement layer.

The design of the Virginia Smart Road pavement sections is summarized in Table 1. Seven of the 12 flexible pavement sections are located on a fill, while the remaining five sections are located in a cut. Each section

is composed of different layers, all having designations in accordance with the Virginia Department of Transportation specifications. The different layers are:

- Seven different wearing surfaces were used (SM-9.5A, SM-9.5A with high laboratory compaction, SM-9.5D, SM-9.5E, SM-12.5D, SMA-12.5, and open-graded friction course (OGFC)). All mixes, with the exception of the OGFC, were constructed at a thickness of 38mm.
- Intermediate hot-mix-asphalt (HMA) base layer, designated BM-25.0, was placed at different thicknesses ranging from 100 to 244mm.
- Three sections have the SM9.5A fine mix placed under the BM-25.0 to examine the benefits of such a design on reducing fatigue cracking.
- Open Graded Drainage Layer (OGDL) was built into nine of the 12 sections (three sections were built without OGDL). Seven sections were treated with asphalt cement, and two were treated with Portland cement. The thickness of this layer is kept constant at 75mm throughout the project.
- Cement Stabilized base, termed as 21-A layer, was used in 10 sections at a thickness of 150mm. The added cement is around 3.5% by weight.
- Subbase aggregate layer, designated as 21-B, was placed over the subgrade at different thicknesses ranging from 75 to 150mm.

**Table 1: Pavement Sections at the Virginia Smart Road**

Section	Length (m)	Wearing Surface (38mm)	BASE BM-25.0 (mm)	BASE SM-9.5A (mm)	OGDL (mm)	21-A Aggr. Cem. Stab. (mm)	21-B Aggr. (mm)
A	104	SM-12.5D/CP	150/CP	0	75/CP	150/CP	175/CP
B	90	SM-9.5D/CP	150	0	75	150	175/ GT/CP
C	87	SM-9.5E/CP	150/CP	0	75	150	175/ GT
D	117	SM-9.5A/CP	150/CP	0	75	150/CP	175/ GT
E	76	SM-9.5D	225/CP	0	0	150	75/ GT/CP
F	94	SM-9.5D	150/CP	0	0	150/CP	150/CP
G	90	SM-9.5D	100/CP	50/CP	0	150	150/ GT/CP
H	90	SM-9.5D	100	50/CP	75/CP	150	75
I	98	SM-9.5A*/CP	100/CP/GM	50	75/CP	150	75
J	92	SM-9.5D	225	0	75/SR/CP	0/GT	150/CP
K	86	OGFC^	244/SR/CP	0	75/CP	0/GT	150
L	104	SMA-12.5/CP	150/GM	0	75/CP	150	75

CP: Copper plate

SR: Stress Relief Geosynthetic

^ 19-mm-thick OGFC over 19-mm SM-9.5D

\* High lab compaction

GT: Woven Geotextile/Separator

GM: Galvanized Metal Mesh

The continuously reinforced concrete pavement section was constructed using a 250-mm thick concrete slab placed over a 75mm OGDL, 150mm 21A layer, and 75mm aggregate layer. The reinforcement within the continuously reinforced concrete slab consisted of #20 longitudinal reinforcing bars and #15 transverse reinforcing bars. The longitudinal reinforcing bars were placed at intervals of 165mm on center. The transverse reinforcement was placed at intervals of 1.2m on center.

The Virginia Smart Road offers a good opportunity to explore the reliability of GPR in measuring layer thickness and monitoring pavement performance over time. To achieve this objective, 31 copper plates were embedded in the flexible pavement during construction. These plates were inserted at the bottom of different layers, and four plates were placed underneath the concrete slab in the rigid pavement. Copper with a conductivity of  $5.7 \times 10^7$  S/m is considered an excellent conductor, and therefore was chosen to serve as a perfect EM reflecting material. Copper sheets (914 × 1219 × 0.7 mm) were placed at several locations in all tested sections as presented in Table 1; Figure 1 shows a copper plate placed on top of subgrade in section B. The copper plates are beneficial in that they indicate where the interface between each two layers occurs. In fact, because some of the pavement

materials do not have significant differences in their dielectric properties, a small amount of energy is reflected back from their interface. This reflected energy is further attenuated by the layers and thus it is obscured by the GPR receiver noise. In this case, accurate determination of the interface becomes difficult.

After completion of the Virginia Smart Road construction, two methods were used to verify that the as-built layer thicknesses conformed to the design. The first method was based on the copper plates. In fact, during the construction of the Virginia Smart Road, the positions of the copper plates were surveyed in the  $x$ ,  $y$ , and  $z$  directions before placement. The layer thicknesses near the copper plates were later determined based on the  $z$  coordinates of the plates. The second method was a direct measurement of the layer thicknesses from cores taken from the road (approximately 120 cores). These two methods showed that the overall error of the HMA layer thickness was around  $\pm 7\%$ .



**Figure 1: Copper plate under 21-B material in section B.**

## GPR SYSTEM

The GPR system used in this research was a SIR-10B system manufactured by Geophysical Survey Systems, Inc. (GSSI). The SIR-10B is an impulse GPR system having two Input/Output channels allowing the connection of two sets of antennae simultaneously.

Two types of antennae were used in this research: an air-coupled antenna and a ground-coupled antenna with a system connected to each channel. The air-coupled system was composed of a pair of separate horn antennae (one serves as a transmitter and the other as a receiver) having a frequency bandwidth of 1 GHz corresponding to a pulse width of 1ns. The ground-coupled system comprised a monostatic bowtie antenna (operating as transmitter and receiver) having a frequency bandwidth of 900 MHz, which corresponds to a pulse width of 1.1ns.

As depicted in Figure 2a, the two types of antennae were mounted behind the GPR survey van, with the control unit set inside of it. This configuration allows data collection by both systems at the same time. To prevent interference from the ground-coupled antenna while collecting data with the air-coupled antenna, the ground-coupled antenna was placed away from the footprint of the air-coupled antenna.

To precisely locate the collected data longitudinally on the road, a distance-measuring instrument (DMI) connected to the survey vehicle wheel was used to control the trigger pulses generated by the GPR pulse generator, as shown in Figure 2b. In this case, data was collected as a function of distance (i.e.,  $n$  scans every meter) rather than as a function of time (i.e.,  $n$  scans every second).



(a)



(b)

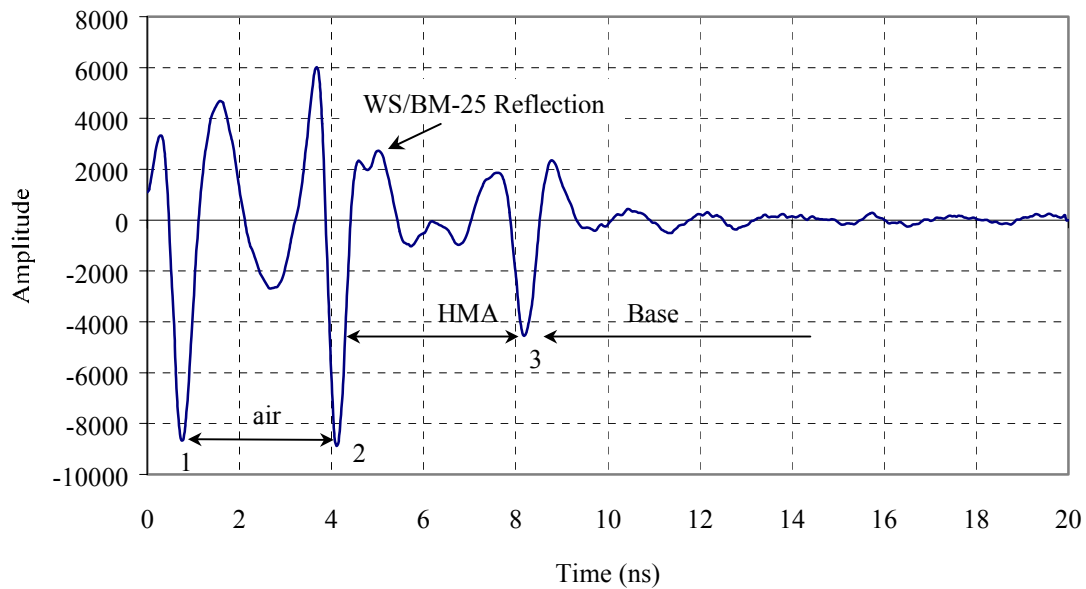
**Figure 2: (a) GPR Survey Van Showing the Air-Coupled and Ground-Coupled Antennas, (b) Distance Measuring Sensor.**

### **GPR DETECTION LIMITATIONS**

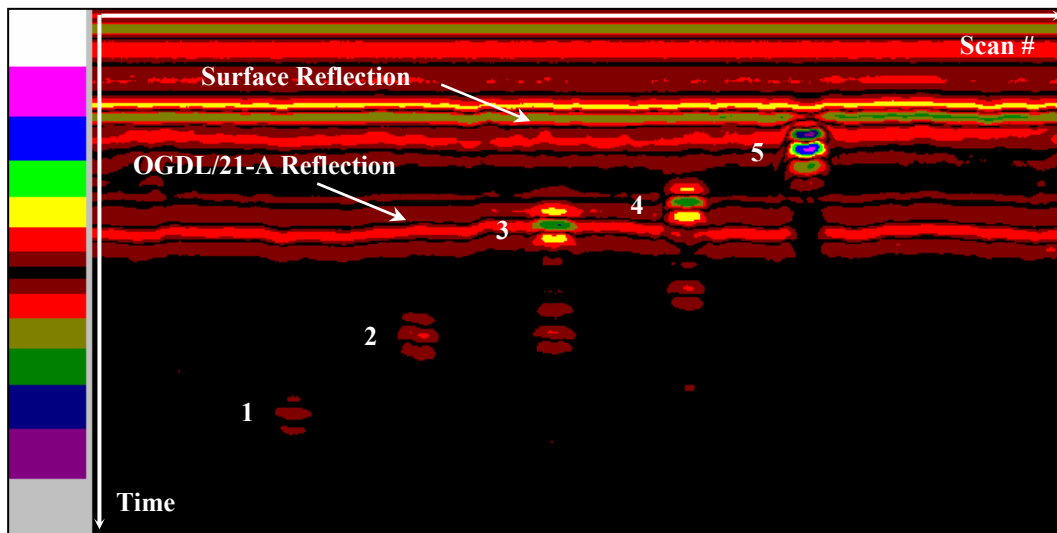
To study the GPR detection limitations, data collected with the air-coupled antenna (usually used for pavement thickness measurement) from section A at the Virginia Smart Road was examined. Figure 3a shows a scope view of a single scan, and Figure 3b illustrates a linescan view of a group of scans collected over section A. A linescan view represents a set of along-track scans stacked together vertically. The amplitude of each scan is quantized and coded into a solid color. Therefore, the x-axis in this figure represents the scan number, which is proportional to the surveyed distance; the y-axis represents the reflection time that can be converted to depth, knowing the dielectric properties of each layer. The amplitude to color transformation function used to obtain Figure 3b is given at the left side of the figure. In order to enhance low reflections, a nonlinear transformation function was used with black representing reflections near zero, bright colors representing positive reflections, and dark colors representing negative reflections.

Three pulses are visible in Figure 3a: (1) the direct coupling pulse between transmitting and receiving antennae, (2) the surface reflection, and (3) the reflection from the OGD/21A interface. In Figure 3b, five strong

reflections can be distinguished. Those correspond to the five copper plates placed at the wearing surface/BM-25.0, BM-25.0/OGDL, OGDL/21-A, 21-A/21-B, and 21-B/subgrade interfaces, respectively.



(a)



(b)

**Figure 3: (a) Scope View of a Scan over Section A, where the Coupling Pulse (1), Surface Reflection (2), and OGDL/21-A Interface Reflection (3) are Visible;**

**(b) Linescan View over Section A showing the Copper Plate Reflections at the (1) 21-B/ Subgrade, (2) 21-A/21-B, (3) OGDL/21-A, (4) BM-25.0/OGDL, and (5) WS/BM-25.0 interfaces.**

It is clear from Figures 3a and 3b that the 21-B/subgrade and 21-A/21-B interfaces are not detectable under normal conditions (i.e., without copper plates). This is due to the low contrast between the dielectric properties of subgrade, 21-B, and 21-A layer, since they were constructed using the same type of limestone material (which has a dielectric constant,  $\epsilon_r$ , of approximately 8). The low contrast in dielectric constant results in a low amplitude reflected signal, which is further attenuated because of material loss. Therefore, the reflected signal collected from

these interfaces is obscured by the receiver noise. The effect of material loss on the reflected signal can be further shown in Figure 3b, where the reflected signal from the deeper copper plates has lower amplitude than the reflected signal from the shallower plates. On the other hand, as illustrated in Figures 3a and 3b, the OGDL/21-A interface is easily detectable even without the copper plate at the interface. This is due to the relatively high contrast between the dielectric constant of HMA ( $\epsilon_r$  approximately 4) and limestone aggregate ( $\epsilon_r$  approximately 8), which results in a high amplitude reflected signal.

According to the design of section A, the HMA layer is composed of a wearing surface, a HMA base layer (BM-25.0) and an asphalt-treated drainage layer (OGDL). However, in Figures 3a and 3b it is not obvious where the reflections from these interfaces occur. In fact, a close examination of Figure 3a shows only a small distortion at the trailing edge of pulse (2), which is not present at the original transmitted pulse depicted in Figure 4a. This distortion is due to the overlap between the surface reflection and the reflection at the wearing surface/BM-25.0 interface. Consequently, in this case, the reflections within the HMA layer are masked by the stronger reflections in their vicinity (surface reflection) rather than by the receiver noise. It should be noted that the location of the distortion does not give a reliable estimate of the interface reflection position. In fact, Figure 4b depicts another scan collected over section A where the distortion disappeared due to the complete overlap between the surface reflection and the wearing surface/BM-25.0 interface reflection. Furthermore, estimation of the wearing surface thickness at this location from the time domain signal depicted in Figure 3a (utilizing the typically used distortion as the interface location, the two-way travel time  $t = 0.93\text{ns}$  and  $\epsilon_r = 3.85$ ) gives a thickness of 71mm, which is much greater than the actual layer thickness (38mm).

The minimum detectable layer thickness insuring a non-overlap between two consecutive reflections is known as the depth (or range) resolution. The depth resolution,  $\Delta d$ , is given by the following equation:

$$\Delta d = \frac{cT}{2\sqrt{\epsilon_r}} \quad (1)$$

where  $c$  is the speed of light in free space ( $c = 3 \times 10^8$  m/s),  $T$  is the transmitted pulse width, and  $\epsilon_r$  is the dielectric constant of the considered layer. For the air-coupled antenna  $T = 1\text{ns}$ , thus for HMA ( $\epsilon_r$  approximately 4), the minimum detectable thickness is around 75mm, which is greater than the 38mm wearing surface thickness.

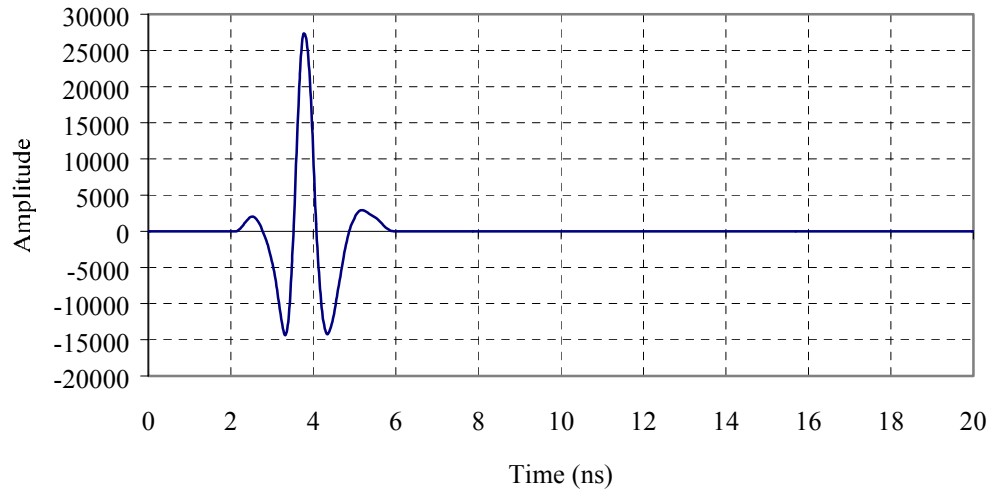
### ACCURACY OF LAYER THICKNESS ESTIMATION USING TIME DOMAIN ANALYSIS TECHNIQUES

For an impulse GPR system, measuring the two-way travel time,  $\Delta t$ , between the two interfaces of a homogeneous layer and knowing the EM velocity  $v$  in (or dielectric constant  $\epsilon_r$  of) the traversed medium yields the thickness  $d$  of the layer as given by equation 2. The two-way travel time is the time that the wave takes to go from one interface to the other and back. It corresponds to the time difference between two consecutive reflected pulses in the GPR collected signal.

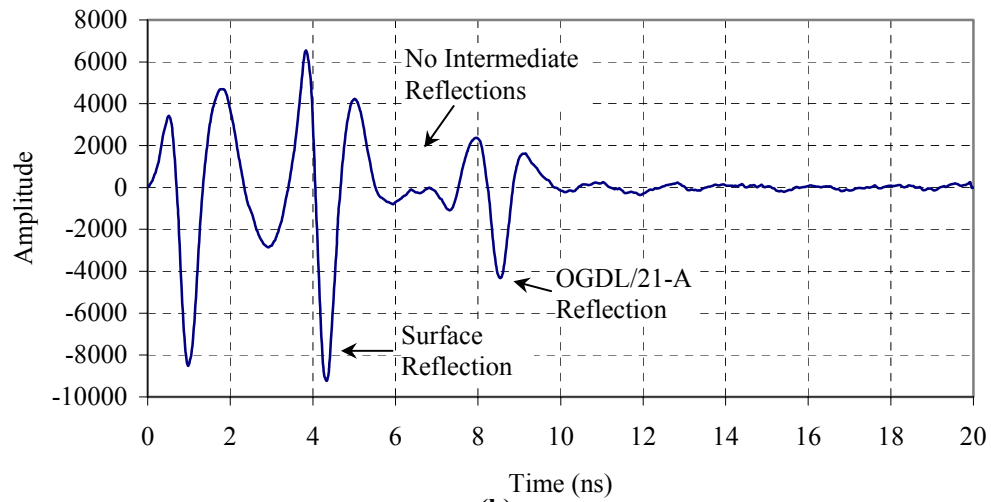
$$d = \frac{v\Delta t}{2} = \frac{c\Delta t}{2\sqrt{\epsilon_r}} \quad (2)$$

The first difficulty in GPR data interpretation when attempting to measure the thickness of a layer is illustrated by the above equation. Specifically, even if it is assumed that the two-way travel time  $\Delta t$  can be accurately measured from the GPR signal, the dielectric constant of the material remains unknown. Even in the case when the individual dielectric constants of different materials used in pavements are known, the dielectric constant of the whole layer is not. In fact, the bulk dielectric constant is greatly affected by moisture content and mixture proportions of the different components of the layer. Therefore, use of a predetermined value for  $\epsilon_r$  can lead to inaccurate thickness estimations.

The simplest technique to overcome this problem is to take calibration cores from the surveyed road and then estimate the dielectric constant from the response near the core locations, knowing the exact thickness at that area (measured from the core). This technique may result in a good estimation of the dielectric constant near the core locations; but may result in an inaccurate result at different locations. The layer dielectric properties usually change from one location to another. The accuracy of this method might be improved by increasing the number of cores taken. However, this may reduce the GPR survey into a destructive technique and therefore jeopardize the whole purpose of using GPR.



(a)



(b)

**Figure 4: (a) Transmitted Pulse from the Air-Coupled Antenna, (b) Scope View of a Second Scan over Section A.**

Another technique was suggested to estimate the dielectric constant from the reflected time domain GPR data (12,13). The method assumes that the pavement is composed of two homogenous layers, namely a HMA layer on top of a base layer. Using principle reflections from both layers (i.e., neglecting any multiple reflections), the dielectric constant of the HMA layer,  $\epsilon_a$ , and that of the base layer,  $\epsilon_b$ , are found according to the following equations:

$$\epsilon_a = \left[ \frac{A_{inc} - A_a}{A_{inc} + A_a} \right]^2 \quad (3)$$

$$\epsilon_b = \epsilon_a \left[ \frac{F - R}{F + R} \right]^2 \quad (4)$$

where,

- $A_{inc}$  is the maximum amplitude of the incident wave. It is obtained by collecting data over a copper plate placed on the surface of the pavement and then taking the negative of the resulting wave.
- $A_a$  is the maximum amplitude reflected from the HMA surface.
- The factor  $F$  is defined as: 
$$F = \frac{4\sqrt{\epsilon_a}}{1 - \epsilon_a}$$
- $R$  is the ratio of the maximum reflected amplitude from the top of the base layer to the maximum reflected amplitude from the top of the HMA layer.

Equations 3 and 4 assume that the dielectric constants of the layers are independent of frequency in the bandwidth of the GPR. Moreover, any attenuation in the HMA layer is neglected, which will mainly affect the value of  $\epsilon_b$ .

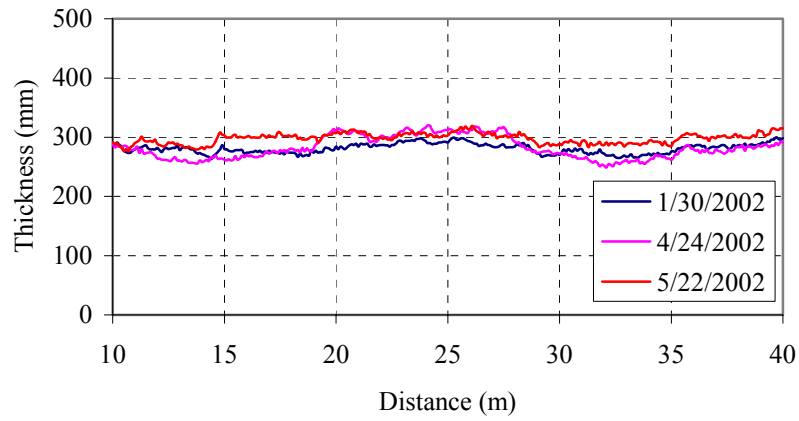
The aforementioned time domain analysis technique was applied to some of the data collected from the Virginia Smart Road. To check the accuracy and the repeatability of the results obtained by this method, data was collected over segments from sections A through G, each averaging 25m in length. Data collection was performed over the same segments during three different surveys (January 30<sup>th</sup>, April 24<sup>th</sup>, and May 22<sup>nd</sup>, 2002) at a spatial resolution of 10 scans/m. Use of a high resolution DMI sensor during the surveys insured that data was collected from exactly the same locations during each survey. During the three surveys, it was expected that the pavement would have different moisture conditions, and therefore the GPR reflected signals would differ. However, the estimated layer thicknesses should remain the same as data was collected over the same locations.

As discussed earlier, due to the low dielectric contrast between the base and subgrade layers, the reflected signal from that interface was not detectable by GPR in any of the seven sections. Consequently the base layer thickness was not estimated from the GPR data. The HMA thicknesses found for each section and for each survey date are illustrated in Figures 5 through 7. These figures show that for the same section, there was a small difference between the thicknesses found from each survey. This difference does not have a specific trend. To check the significance of the difference between the thicknesses determined by the different surveys, the root-mean square error (RMSE) between any two sets of thickness (i.e., between survey 1 and 2, survey 1 and 3, and survey 2 and 3) was computed for each section. Table 2 presents the maximum RMSE found for each section along with the average HMA thickness estimated by each survey, and the maximum expected HMA thickness based on the pavement original design and corrected by the correction factor found from control cores. For comparison purposes, the percent values of the RMSE were computed with respect to the average thicknesses found for January 30<sup>th</sup> for each section. According to Table 2, all layer thicknesses were slightly overestimated for the three surveys and for all the seven sections. Furthermore, the RMSE was around 7% for sections A through E (lowest was 5.6% for section D and highest was 12.4% for section G).

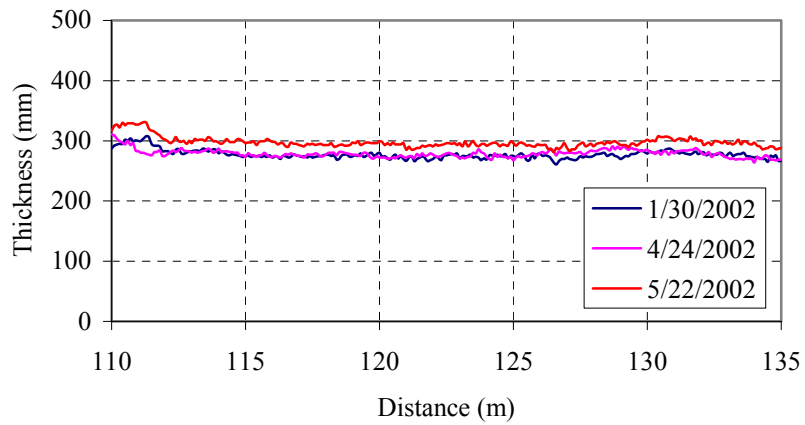
**Table 2: HMA Thicknesses Found by GPR for the Three Survey Dates**

Section	Design Thickness (mm)	Maximum Thickness* (mm)	Average Thickness on 1/30/02 (mm)	Average Thickness on 4/24/02 (mm)	Average Thickness on 5/22/02 (mm)	Max RMSE between three surveys (%)
A	263	281	281	282	298	7.6
B	263	281	277	279	298	7.5
C	263	281	264	273	282	6.9
D	263	281	269	273	283	5.6
E	263	281	286	287	302	7.2
F	188	201	213	224	226	9.1
G	188	201	196	213	208	12.4

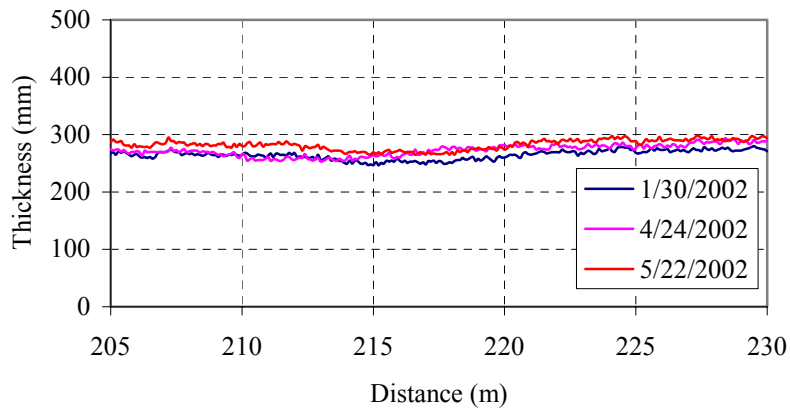
\* Maximum expected thickness = design thickness increased by 7% error.



(a)

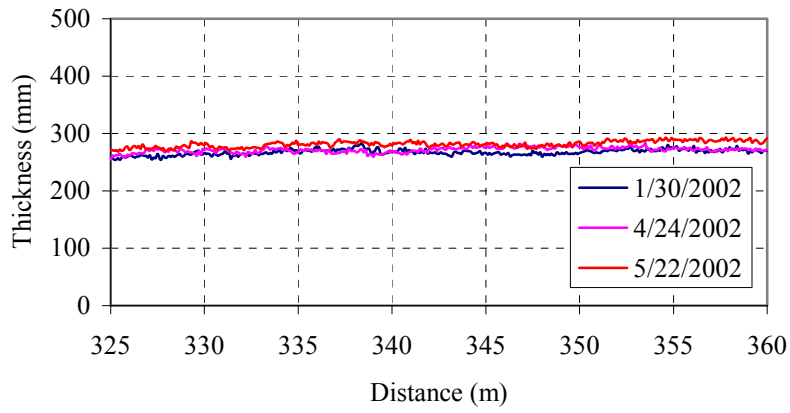


(b)

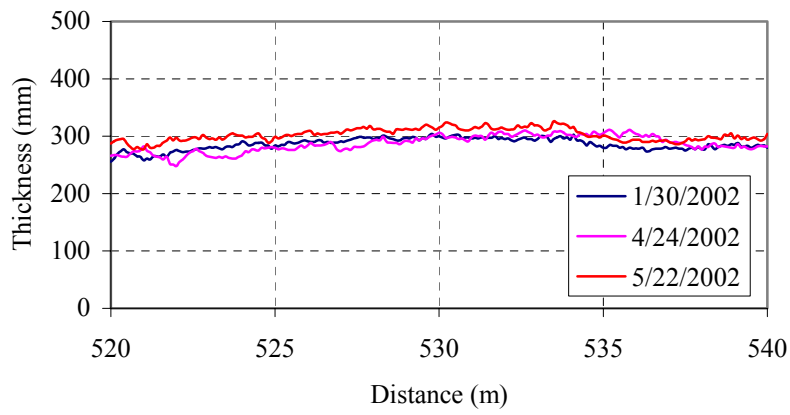


(c)

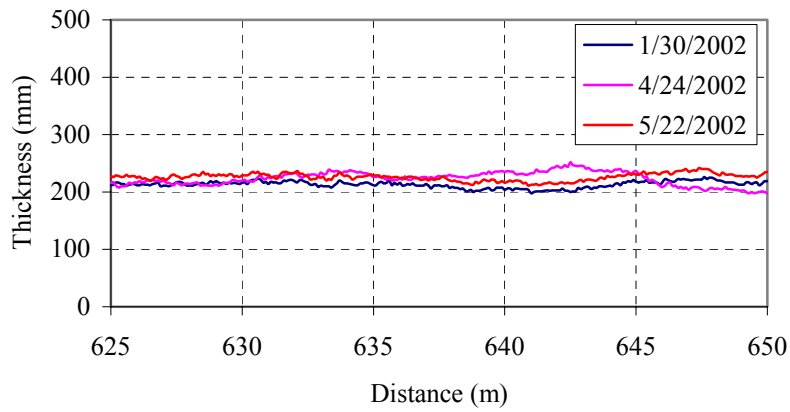
Figure 5: HMA Layer Thicknesses Found by GPR for Sections: (a) A, (b) B, and (c) C.



(a)



(b)



(c)

Figure 6: HMA Layer Thicknesses Found by GPR for Sections: (a) D, (b) E, and (c) F.

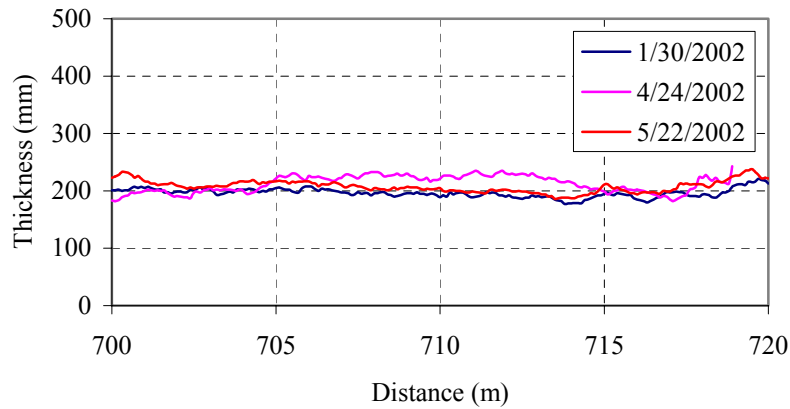


**Figure 7: HMA Layer Thicknesses Found by GPR for Section G.**

The overestimation of the HMA layer thickness could be explained by the assumptions made in computing the HMA dielectric constant. In fact, as given by equation 2, the HMA dielectric constant is estimated only by the surface reflection. Therefore, the method assumes that the HMA layer is composed of the same material (i.e., constant  $\epsilon_a$ ) throughout its entire thickness. This assumption does not hold for the Virginia Smart Road sections as was illustrated in Table 1. The received GPR signal is unable to discriminate between the presence of different mixes within the HMA layer. The HMA dielectric constant estimated from the surface would be different from the overall dielectric constant. In addition, based on the complex refractive index model mixture law, the dielectric constant of the HMA base would be higher than that of the wearing surface HMA because the latter has less aggregate and more asphalt than the base mix (13). Consistent with the same mixture law, the overall HMA dielectric constant would be greater than that of the surface, especially if limestone aggregate is used. Therefore, the layer thickness found by the surface dielectric constant is expected to be overestimated due to the inverse proportionality between dielectric constant and layer thickness as shown in equation 2.

The small variability between the different surveys could be also attributed to the errors in estimating the HMA dielectric constant. In fact, any variability of the moisture content of the subsurface layers would affect the two-way travel time of the GPR electromagnetic signals. If this effect is not taken into account in the estimation of the HMA dielectric constant, errors would be introduced in the conversion from travel time to layer thicknesses using equation 2.

#### **PAVEMENT THICKNESS ESTIMATION USING COMMON MIDPOINT TECHNIQUE**

As was shown above, estimation of the dielectric constant of the HMA layer based on the surface reflection does not yield accurate thickness results for an inhomogeneous HMA layer (i.e., composed of multiple layers). To overcome this problem, an average value of the dielectric constant throughout the layer should be used. This improvement could be achieved using a common midpoint technique as illustrated in Figure 8a. In this case, the HMA layer dielectric constant is computed based on the reflection times  $t_1$  and  $t_2$  obtained respectively from a monostatic and a bistatic antenna. The layer dielectric constant,  $\epsilon_r$ , is computed according to equation 5:

$$\epsilon_r = \frac{c^2(t_2^2 - t_1^2)}{x^2} \quad (5)$$

where  $c$  is the speed of light in free space and  $x$  is the distance between the two antennas of the bistatic system. It should be noted that because the HMA dielectric constant is determined from the reflections at the bottom of the layer, it represents an average value and therefore accounts for any inhomogeneities within the layer.

The configuration depicted in Figure 8a could be modified to suit the antenna configuration of the GPR system used for this research (i.e., a bistatic air-coupled antenna system and a monostatic ground-coupled antenna, Figure 2a) as shown in Figure 8b. The layer dielectric constant is then found after solving for the incidence and

transmission angles,  $\theta_i$  and  $\theta_t$ , and the distance  $x_1$ , knowing the two-way travel times  $t_1$  and  $t_2$  (computed from the ground-coupled and air-coupled responses, respectively), the distance  $x_0$  between the bistatic transmitter and receiver, and the height  $d_0$  of the air-coupled system above ground. A simple algorithm could be used to estimate the HMA dielectric constant using the second configuration:

1. Estimate the reflection times  $t_1$  and  $t_2$  corresponding to the two-way travel times in the HMA layer obtained by the ground-coupled and air-coupled systems, respectively.
2. Calculate the transmission angle  $\theta_t$  using the following equation:

$$\tan \theta_t = \frac{\sqrt{t_2^2 - t_1^2}}{t_1} \quad (6)$$

3. Find the angle of incidence  $\theta_i$  by solving numerically the following equation:

$$2d_0 \tan \theta_i + c \frac{\sin \theta_t}{\sin \theta_i} \sqrt{t_2^2 - t_1^2} = x_0 \quad (7)$$

4. Compute the HMA dielectric constant  $\epsilon_a$  using the following equation:

$$\epsilon_a = \left( \frac{\sin \theta_i}{\sin \theta_t} \right)^2 \quad (8)$$

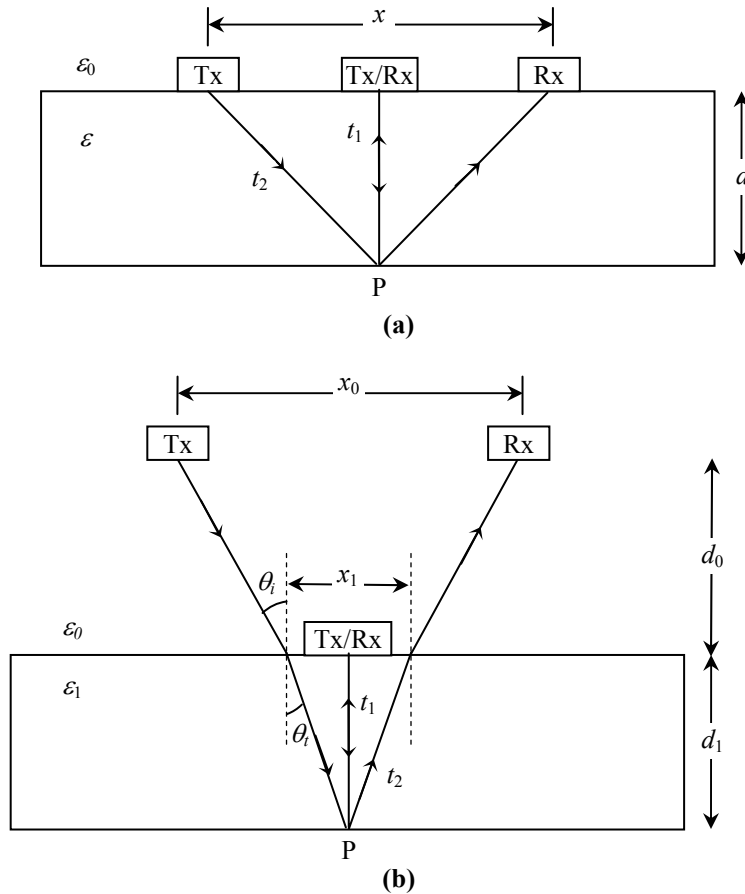


Figure 8: (a) Common Midpoint Configuration, (b) Modified Common Midpoint Configuration.

The performance of this data analysis technique is still under investigation using data from the Virginia Smart Road. However, preliminary results have shown that it outperforms the classic time domain technique. In fact, this technique was used to analyze the GPR data collected from a 17-mile, 4-lane section of interstate I-81. Comparison of the results of this technique with test cores showed an average absolute error of 6.8% (4). The same data was analyzed using the classic time domain technique and showed an average absolute error of 12.7%. A summary of the results found by both techniques is presented in Table 3.

## CONCLUSIONS

This study identified some of the problems arising from GPR data interpretation for estimating pavement layer thickness. The study was based on data collected from an experimental pavement system, the Virginia Smart Road and I-81. It was shown that a GPR system cannot detect layer interfaces unless a significant contrast in the dielectric constants exists between the two considered layers. This requirement is more important for the deeper interfaces because of material loss that further attenuates the GPR electromagnetic signals. Moreover, it was verified that depending on the dielectric properties of a layer and the pulse width of the GPR system used, there exists a minimum thickness (known as depth resolution) that could be reliably detected by GPR. The depth resolution could be improved by using signal processing procedures such as deconvolution. In addition, prior information about the studied pavement structure is usually beneficial for GPR surveys in order to predict what could be detected by the GPR. In general, Time domain analysis techniques of GPR data based on the reflection amplitudes have been proven inaccurate. Therefore, these techniques should be used only for applications where a relatively low level of accuracy is required. More sophisticated techniques could be used to improve the results accuracy at the expense of a higher computation time. These techniques are still under investigation using data from the Virginia Smart Road. Preliminary evaluation of such techniques on data collected from interstate I-81 revealed an error of 6.8%, whereas the classic time domain technique showed an error of 12.7% for the same data.

**Table 3: Correlation between Core Thickness and GPR Thickness for I-81 Data**

Core #	Core Location *	Core Thickness (mm)	GPR Thickness (mm) CMP Method	GPR Thickness (mm) Classic Method	Absolute Error (%) CMP Method	Absolute Error (%) Classic Method
1n	7.00	337	322	378	4.3	12.1
2n	9.00	311	303	399	2.6	28.4
3n	11.00	368	350	459	5.0	24.6
4n	12.90	343	322	377	6.1	10.0
5n	14.00	330	359	374	8.7	13.3
6n	15.50	298	274	272	8.2	8.8
7n	16.45	279	310	322	11.0	15.5
8s	16.00	305	313	311	2.7	1.8
9s	15.40	267	308	324	15.5	21.3
11s	15.22	267	296	306	11.0	14.5
14s	14.95	286	283	315	1.0	10.1
17s	14.68	292	303	301	3.7	2.9
21s	10.64	375	345	405	7.9	8.1
22s	7.00	356	331	377	6.9	5.8
<b>Mean Error (%)</b>					<b>6.8</b>	<b>12.7</b>

\* Core Location in county milepost

**REFERENCES**

1. Scullion, T., Lau, C. L., and Chen, Y. (1994). *Implementation of the Texas ground penetrating radar system* (Research Report 1233-1). Texas Transportation Institute.
2. Davis, J. L., Rossiter, J. R., Mesher, D. E., and Dawley, C. B. (1994). Quantitative assessment of pavement structures using radar. *Proceedings of the 5<sup>th</sup> International Conference on Ground Penetrating Radar*, 319-334.
3. Maser, K. R. (1996, February). Measurement of as-built conditions using ground penetrating radar. In P. E. Hartbrower and P. J. Stolarski (Eds.), *Structural Materials Technology: An NDT Conference* (pp. 61-67).
4. Lahouar, S., Al-Qadi, I. L., Loulizi, A., Trenton, C. M., and Lee, D. T., *Development of an Approach to Determine In-Situ Dielectric Constant of Pavements and Its Successful Implementation at Interstate 81*, The 81<sup>st</sup> Transportation Research Board Annual Meeting, Paper No. 02-2596, Washington DC, January 13-17, 2002.
5. D'Angelo, J. A. (1986), *Portland cement concrete pavement stabilization*. Federal Highway Administration: Washington, DC.
6. Sheftick, D. E., and Bartoski, T. A. (1997). *Study of void detection methods and slab stabilization procedures* (Research Project 86-102). Pennsylvania Department of Transportation, Bureau of Construction and Materials.
7. Al-Qadi, I. L. (1997). The penetration of electromagnetic waves into hot-mix asphalt. *Proceedings of the Nondestructive Evaluation of Civil Structures and Materials* (pp. 195-209). Boulder, CO.
8. Rmeili, E. and Scullion, T. (1997). *Detecting stripping in asphalt concrete layers using ground penetrating radar* (Paper No. 97-0508). Transportation Research Board, Washington, DC.
9. Al-Qadi, I. L. and Loulizi, A. (1999, June). *Using GPR to evaluate the effectiveness of moisture barriers in pavements*. In M. C. Forde (Ed.), *Structural Faults and Repair 99, 8<sup>th</sup> International Conference*, London, England.
10. Loulizi, A., Al-Qadi, I. L., Bhutta, S., and Flintsch, G. (1999). Evaluation of geosynthetics when used as separators (Paper No. 99-1316). *Transportation Research Record, Geotechnical Aspects of Pavements, 1687*, 104-111.
11. Al-Qadi, I. L., Nassar, W. M., Loulizi, A., Flintsch, G. W, and Freeman, T. (2000, January). *Flexible pavement instrumentation at the Virginia Smart Road* (Paper No. 001275). The 79th Transportation Research Board Annual Meeting, Washington, DC.
12. Wimsatt, A. J., Scullion, T., Ragsdale, J., and Servos, S. (1998). *The use of ground penetrating radar data in pavement rehabilitation strategy selection and pavement condition assessment*. Washington, DC: Transportation Research Board.
13. Maser, R. M. and Scullion, T. (1992). Automated pavement subsurface profiling using radar: Case studies of four experimental field sites. *Transportation Research Record, 1344*, 148-154.